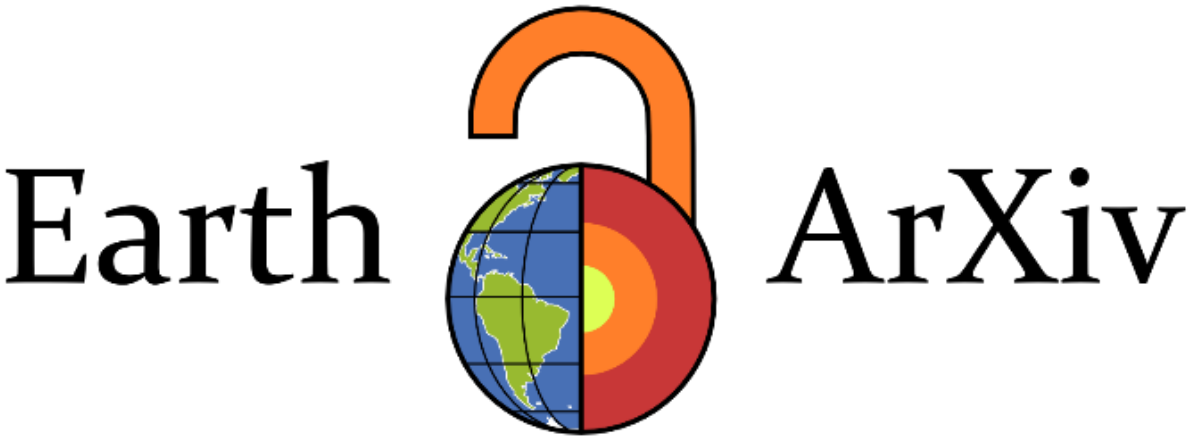

Satellite Embedding: A Review

Longhao Wang[a,b,*]

[a]*Key Laboratory of Water Cycle and Related Land Surface Processes, Institute of Geographic Sciences and Natural Resources Research, Chinese Academy of Sciences, Beijing, 100101, China*
[b]*University of Chinese Academy of Sciences, Beijing, 100049, China*

Abstract

Satellite embeddings have become a practical interface between large-scale Earth observation data and downstream geospatial analysis, yet the literature is still organized mainly around foundation models rather than the embeddings they produce. This review reframes the area from an embedding-centered perspective. We first define satellite embeddings as reusable latent representations derived from satellite or multimodal Earth observation data, and organize existing methods along three axes: model family, data and modality support, and deployment mode. We then consolidate 19 representative models into a unified dossier covering publication source, authorship, spatial scale, temporal semantics, architecture, pretraining signal, embedding dimensionality, runtime behavior, and code or artifact availability. Building on the organization of recent remote sensing reviews, we connect the model taxonomy to application requirements, data regimes, output granularity, and operational constraints. We further report a compact Wuhan benchmark that evaluates frozen embeddings on classification, fraction regression, water extraction, and dense segmentation within a shared 500 m grid. The resulting review is intended to serve as both a technical reference and an evidence-backed evaluation framework for selecting satellite embeddings in practical Earth observation workflows.

Keywords: Satellite embeddings, Earth observation, Remote sensing foundation models, Representation learning, Geospatial benchmarks, Model evaluation

*Corresponding author.
Email address: wanglonghao0857@igsnrr.ac.cn (Longhao Wang)

1. Introduction

Earth observation is entering a representation-first stage. Open satellite constellations, long-running public archives, and large pretraining corpora have accelerated the development of remote sensing foundation models, while recent surveys have documented a rapid shift from vision-only pretraining pipelines toward multimodal, generalist, and task-adaptive Earth observation systems [1–3]. By 2025, models such as SkySense++ were already reporting consistent gains across classification, detection, and segmentation on 12 Earth observation tasks in 7 domains, illustrating how quickly the field is moving from narrow benchmark models toward reusable geospatial representations [4]. At the same time, new productized representations such as GSE and TESSERA suggest that the field is no longer defined only by trainable checkpoints; it is increasingly also defined by reusable embedding layers that can be queried, indexed, and redistributed as geospatial products [5, 6].

This recent surge did not emerge in isolation. Satellite embeddings inherit a longer remote sensing representation-learning trajectory that begins well before the current foundation-model vocabulary. Earlier Earth observation pipelines were dominated by hand-crafted spectral indices, texture descriptors, bag-of-visual-words features, and shallow classifiers designed for scene classification, land-cover mapping, or target detection. The first major break came when convolutional neural networks were transferred from natural images into remote sensing, making it possible to learn hierarchical spatial features directly from high-resolution imagery rather than engineering them manually. Early CNN-based scene classification work showed that transfer learning could outperform traditional remote sensing descriptors and established a practical template for representation reuse in Earth observation [7]. In retrospect, those CNN feature extractors were the immediate ancestors of today's satellite embeddings: users often discarded the final classifier and reused intermediate or pooled activations as generic scene descriptors.

The second break was infrastructural as much as architectural. Free and open satellite archives, especially Landsat and Sentinel, dramatically increased the scale of accessible Earth observation data; platforms such as Google Earth Engine reduced the friction of assembling geographically distributed training corpora; and commodity GPU clusters made it feasible to train larger encoders on longer temporal stacks [8]. These conditions changed the field from one centered on carefully curated benchmark datasets

to one capable of pretraining on global or continental imagery streams. Self-supervised learning then provided the methodological bridge. Seasonal Contrast demonstrated that remote sensing models could be pretrained directly from uncurated satellite time series without dense manual annotation, while the broader success of vision transformers shifted the community toward token-based architectures that scale more naturally with patch representations, masking, and multimodal fusion [9–11]. Once these ingredients were in place, the transition from task-specific CNN encoders to reusable Earth observation representation models became much faster.

The third break was the consolidation of those ingredients into model families that look recognizably "foundation-like" from a remote sensing perspective. Transformer backbones enabled patch masking and reconstruction objectives, as seen in SatMAE and ScaleMAE; contrastive learning made semantic alignment and retrieval practical, as seen in RemoteCLIP; and modality-aware tokenization opened the door to sensor-flexible encoders such as Prithvi, DOFA, Galileo, and later multimodal systems [12–17]. At the same time, product-serving workflows matured: instead of exposing only a checkpoint, some systems began serving annual or static embedding layers that could be sampled directly in mapping pipelines. That shift matters because it changes the unit of use. The operational object is no longer only a model to fine-tune, but also a representation product to query, compare, and fuse with labels or side information.

This evolution is important because remote sensing is not merely another image domain. Earth observation representations must absorb multi-resolution and multi-sensor inputs, spectral bands beyond RGB, repeated observations through time, strong geographic and seasonal dependence, and large shifts in coverage, cloud conditions, and annotation density. As emphasized by recent surveys, the gap between natural-image assumptions and remote sensing practice remains substantial, especially when models are transferred across sensors, regions, and tasks [1–3]. A recent NASA primer makes the same point from a deployment perspective: benchmark scores alone are insufficient for model selection in Earth observation, because practitioners must also reason about pretraining data, tokenization, architectural choices, and downstream use-case fit [18]. In other words, the central question is no longer only whether a remote sensing foundation model exists, but what kind of representation it exposes, under what sensing assumptions, and with what practical trade-offs.

That framing motivates the core viewpoint of this review. In opera-

tional use, practitioners rarely begin with a full training recipe or a backbone diagram. They begin with an *embedding*: a pooled scene vector for classification or retrieval, a dense token grid for segmentation, an annual embedding field for wide-area mapping, or a shared latent space aligned with text and metadata. The same backbone can induce very different reusable objects depending on pooling rules, temporal summarization, modality routing, adapter design, or product distillation. Conversely, models trained with different pretraining objectives can occupy a similar practical niche if both yield compact, transferable representations. This is why contrastive image-text systems such as RemoteCLIP [14], masked autoencoder lineages such as SatMAE and SatMAE++ [12, 19], multimodal generalists such as Prithvi and DOFA [15, 16], and precomputed global embedding products such as GSE and TESSERA [5, 6] should be read not as isolated threads, but as members of a common satellite embedding ecosystem.

An embedding-centered review is also useful because it makes evaluation more realistic. What matters for downstream use is not only whether a model reaches a high score on one benchmark, but whether its representation is robust, spatially appropriate, temporally interpretable, and easy to deploy in real mapping workflows. These issues are becoming more visible as the field matures. REOBench, for example, reports that current Earth observation foundation models can experience substantial degradation under realistic corruptions, with performance drops ranging from less than 1% to more than 20% depending on the task, architecture, and perturbation type [20]. Such evidence reinforces the need for a review that does more than list models. It must connect model families to sensing regimes, output forms, robustness expectations, and application scenarios.

This review therefore adopts an explicitly embedding-centered scope. We focus on reusable latent representations derived from satellite and closely related Earth observation data, rather than on remote sensing foundation models in the abstract. Our aim is to bridge three levels that are often separated in the literature: the model paper, the data-and-task setting, and the benchmark protocol. Concretely, the survey makes four contributions:

(i) it defines a review-specific concept of *satellite embedding* and proposes a unified taxonomy spanning model family, sensing modality, temporal semantics, output granularity, and deployment form;

(ii) it assembles a structured dossier for the 19 canonical models currently exposed in the `rs-embed` workspace, including publication metadata, sup-

ported sensors, spatial resolution, architecture, output dimensionality, and practical deployment characteristics;

(iii) it links the model landscape to application-facing use by organizing downstream tasks, outlining a consistent small-area evaluation protocol, and clarifying where different embedding families are likely to be strong or fragile;

(iv) it reports a compact evidence-backed benchmark over a shared Wuhan ROI, using frozen embeddings and lightweight probes to compare classification, fraction regression, water extraction, and dense segmentation behavior across model families.

The remainder of this paper follows that logic. Section 2 defines the concept and taxonomy of satellite embeddings. Section 3 reorganizes the model landscape into major families and provides a detailed catalog. Sections 4 and 5 move from the review taxonomy to application requirements and comparative evaluation. Sections 6 and 7 discuss open questions and conclusions. The goal throughout is to make the review useful both as a scholarly synthesis and as a practical entry point for researchers who need to select, compare, and deploy satellite embedding models.

2. Overall Landscape of Satellite Embeddings

2.1. Why an embedding-centered review?

Most existing remote sensing foundation model surveys are organized around pretraining paradigms, modality combinations, or downstream tasks. That is useful for describing the broader field, but it is not the most natural entry point for practitioners. In operational use, the object that is actually reused is usually an embedding: a pooled scene vector, a dense token grid, an annual embedding field, or a joint multimodal latent space. This review therefore starts from the reusable representation layer rather than from the training recipe alone.

2.2. What is a satellite embedding?

In this review, a satellite embedding is a reusable latent representation derived from satellite or related Earth observation data and intended to support multiple downstream tasks beyond the pretraining objective. This definition intentionally includes both on-the-fly encoder outputs and precomputed

embedding products. It excludes purely task-specific logits or handcrafted indices unless they are explicitly repackaged as a transferable representation layer.

Four representation forms appear repeatedly in the current literature:

1. **Pooled scene vectors**, commonly exposed by transformer encoders for classification, regression, or similarity search.
2. **Dense token grids**, which preserve local spatial structure and can support segmentation or dense retrieval.
3. **Annual embedding fields**, where the representation is served as a spatial product rather than recomputed at inference time.
4. **Joint multimodal spaces**, where the embedding aligns imagery with text, metadata, or additional sensor streams.

2.3. Field evolution and major design axes

For a remote sensing review, the overall story should appear before the detailed taxonomy. The field has evolved from early optical and masked-reconstruction pipelines toward broader multimodal, temporal, vision-language, and productized embedding systems. Figure 1 provides this overall chronological view, which is easier for readers to absorb than a flat list of models.

We organize the literature along three orthogonal axes.

Model family.. The first axis groups models by how the representation is learned and exposed: precomputed embedding products [5, 6, 21], vision-language systems [14, 22], masked autoencoder derivatives [12, 13, 19], multimodal generalist encoders [15–17, 23–25], and application-specialized Earth observation encoders [26–29].

Data and modality.. The second axis captures the sensing substrate. Current models differ in optical-only versus optical-plus-SAR support, single-scene versus time-series modeling, fixed spectral assumptions versus wavelength-aware adaptation, and fine-resolution surface imagery versus coarse-resolution all-sky or atmosphere-linked sensing.

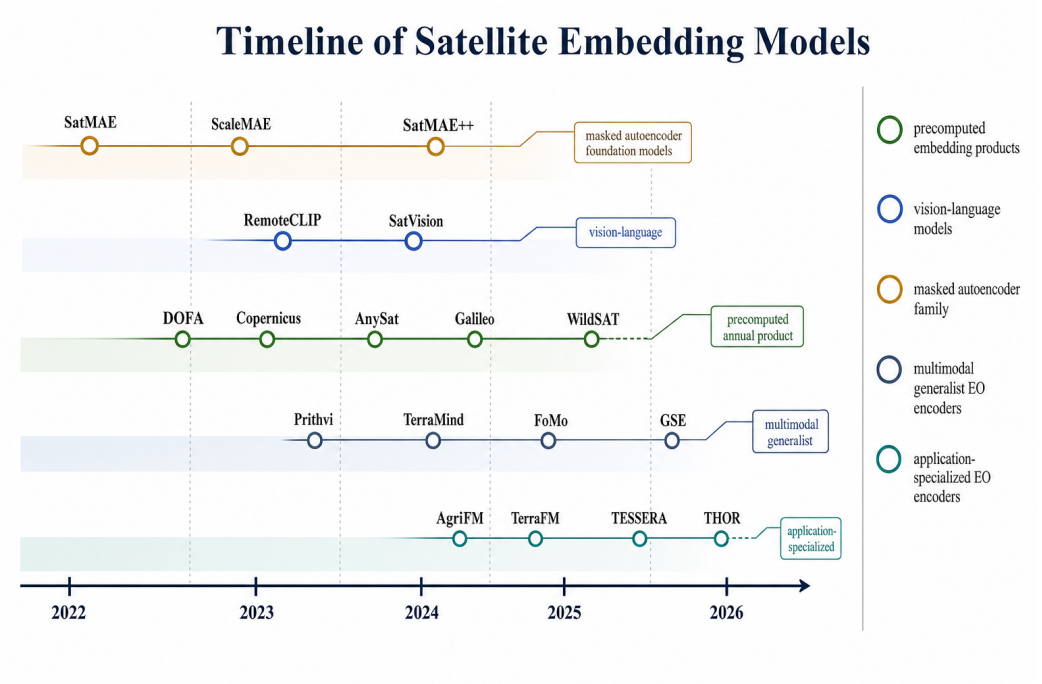

Figure 1: Model timeline view for the satellite embedding landscape. The figure emphasizes how precomputed products, masked autoencoder lineages, multimodal generalists, and application-specific encoders accumulate over time rather than appearing as a single homogeneous wave.

Deployment mode.. The third axis separates systems that run a neural encoder at query time from systems that distribute the embedding directly as a product. This distinction is central for benchmarking because it changes runtime, storage, temporal flexibility, and failure modes. A precomputed product may offer extremely fast access but less temporal control, while an on-the-fly encoder may provide higher flexibility at the cost of data loading and GPU latency.

2.4. Scope of this review

An embedding-centered review should not simply relabel all remote sensing foundation models as satellite embeddings. Instead, the central question is whether the representation can serve as a general interface for downstream use. This criterion explains why annual products such as GSE and TESSERA belong in the same discussion as encoder checkpoints such as SatMAE++,

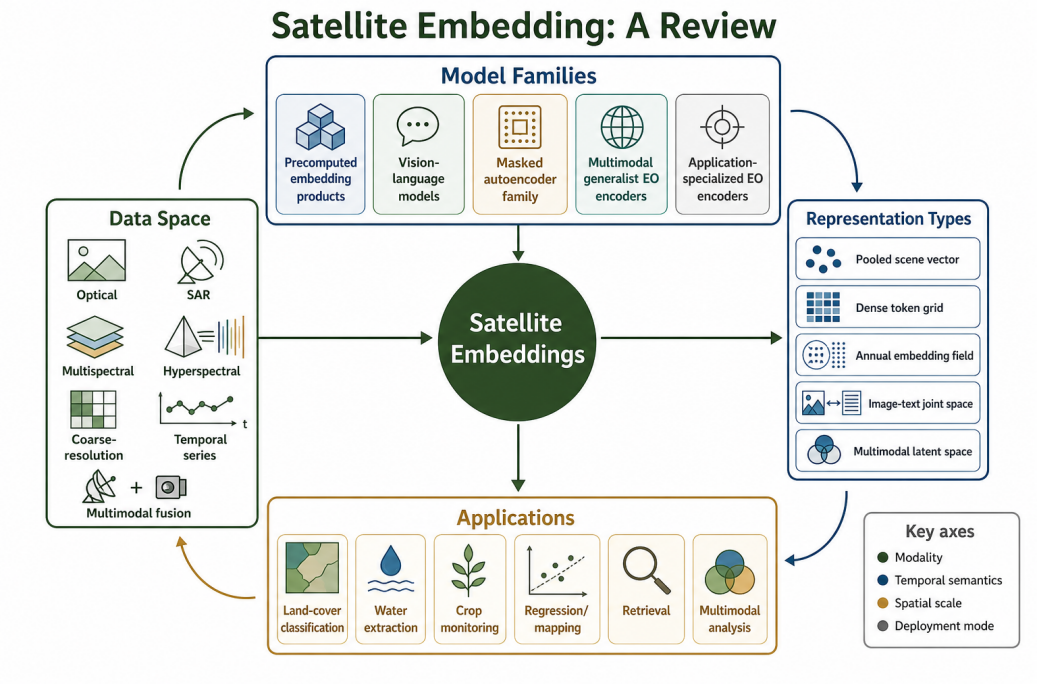

Figure 2: Conceptual map of the satellite embedding landscape. The review is structured around four linked components: data space, model family, representation type, and downstream application. This framing is intentionally embedding-centered rather than checkpoint-centered.

AnySat, or TerraFM. All of them provide a transferable representation layer, but they differ sharply in spatial scale, temporal semantics, and deployment assumptions. Figure 2 summarizes this review logic in one diagram.

3. Model Families of Satellite Embeddings

The current `rs-embed` workspace exposes 19 canonical models, and the accompanying dossier records their publication metadata, supported sensors, output forms, and runtime summaries. For a review article, however, the reader should not face these as a flat inventory. A more natural structure is to first divide the field into a few broad model families, then summarize the common architecture and data logic of each family, and only after that return to a unified comparison table.

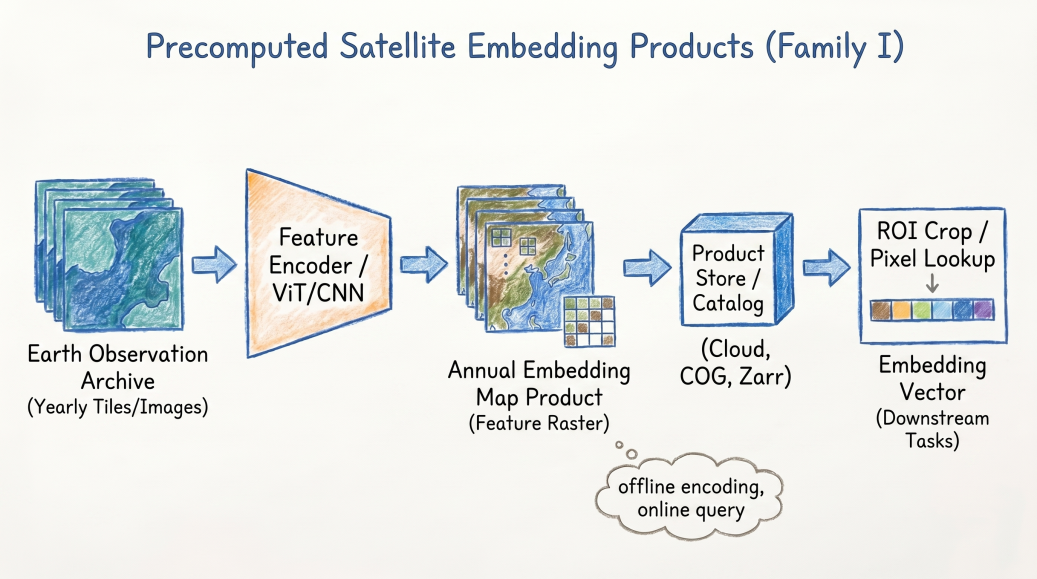

Figure 3: Unified architecture sketch for precomputed embedding products. The dominant pattern is offline large-scale representation learning followed by annual or static embedding map generation, cataloging, and fast ROI-level feature access.

3.1. Family I: Precomputed embedding products

This family treats the embedding itself as a distributed geospatial product rather than as a checkpoint that must be run by the user. Examples include GSE, TESSERA, and Copernicus-style feature maps [5, 6, 21]. Their main strengths are immediate access, large-area consistency, and low inference burden at use time. Their main limitations are temporal rigidity, storage requirements, and dependence on a fixed upstream production workflow.

Architecture summary.. As summarized in Figure 3, the central architectural move is to shift most computation from user-time to production-time. A large Earth observation archive is first condensed into a precomputed feature layer, often annualized or otherwise temporally summarized. Downstream users query that layer by ROI, tile, or pixel rather than rerunning the encoder. This architecture is especially attractive for wide-area monitoring and rapid transfer when access latency matters more than flexible temporal conditioning.

Pseudo-code template..

```
Input:
  Earth observation archive A
  temporal grouping rule T
  query ROI q

Offline stage:
  train encoder f_theta on large EO archive A
  for each period t in T:
      E_t <- f_theta(A_t)
      store embedding map E_t in product catalog

Online stage:
  crop or sample features z <- E_t[q]
  optionally pool or aggregate z
  train lightweight head g on sampled embeddings
  return prediction or retrieved features
```

3.2. Family II: Masked autoencoder and pure vision encoders

This group includes models such as SatMAE, SatMAE++, and Scale-MAE [12, 13, 19]. These methods are usually strongest when the goal is to learn transferable visual structure from optical or multispectral imagery through reconstruction-style pretraining. They are also among the clearest examples of the modern remote sensing foundation model trend, and many later systems can be interpreted as extending this lineage in scale, modality, or temporal handling.

Architecture summary.. The shared logic in Figure 4 is to learn a compact latent representation from partial visual evidence. Randomly masked patches, channels, or scale-aware inputs are passed through a vision encoder, while a reconstruction module encourages the latent space to preserve transferable visual structure. These embeddings often work well for classification and segmentation because they retain strong spatial cues without requiring language supervision.

Pseudo-code template..

```
Input:
  satellite tile x
  masking policy M

visible, hidden <- apply_mask(x, M)
tokens <- patch_embed(visible)
latent <- encoder(tokens)
recon <- decoder(latent, hidden)
loss <- reconstruction_loss(recon, x)
```

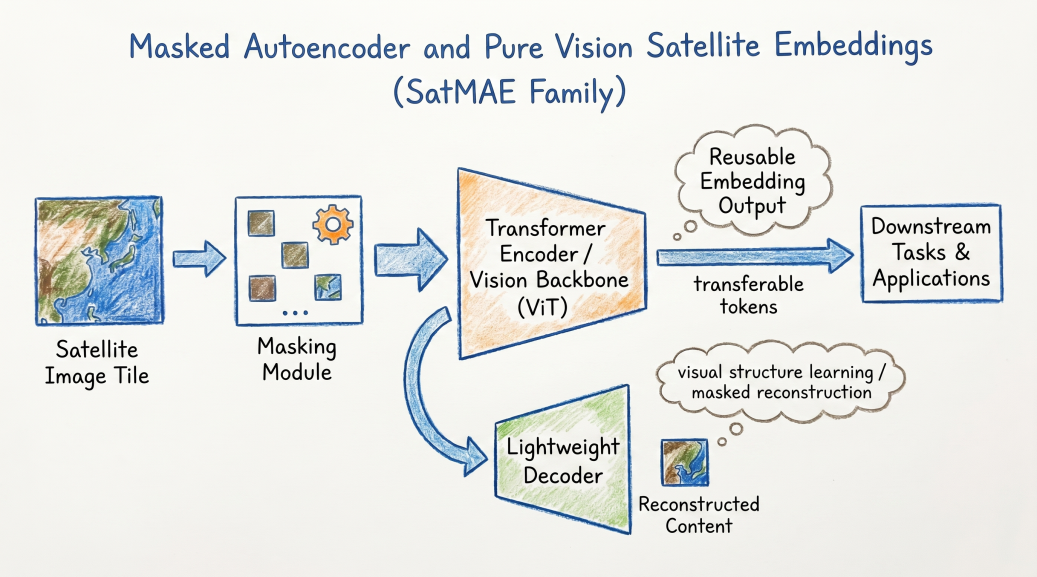

Figure 4: Unified architecture sketch for masked autoencoder and pure vision satellite embedding models. Satellite tiles are partially masked, encoded by a transformer-style vision backbone, and supervised through reconstruction while the latent tokens are reused as transferable embeddings.

```
update model parameters

at inference:
  z_pool, z_grid <- read encoder representations
  return transferable embedding features
```

3.3. Family III: Vision-language and cross-modal embeddings

RemoteCLIP and WildSAT [14, 22] illustrate the main idea of this family: satellite imagery is no longer embedded only against itself, but aligned with text, captions, habitat descriptions, or ecological side observations. Figure 5 shows this shared alignment pattern. This changes the representation from a purely visual latent space into a semantic one, which is why these models are especially important for retrieval, zero-shot transfer, and open-vocabulary interaction.

Architecture summary.. Two encoders, one visual and one language or cross-modal, are trained to bring matched image-text or image-side-information pairs closer in a shared embedding space. The representation becomes useful not just for supervised transfer but also for semantic search and weakly

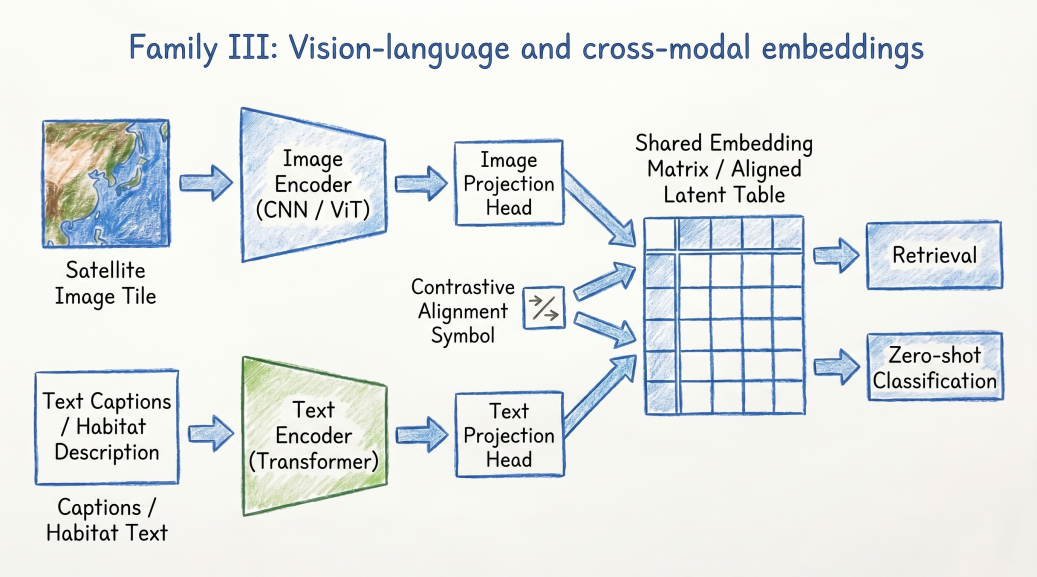

Figure 5: Unified architecture sketch for vision-language and cross-modal satellite embeddings. The core pattern is image and text or ecological side-information encoding into a shared latent space trained by contrastive or alignment objectives.

supervised reasoning. In practice, this family adds a form of interpretability and open-vocabulary access that reconstruction-only models typically lack.

Pseudo-code template..

```
Input:
  satellite image x
  text or side-information y

z_img <- image_encoder(x)
z_txt <- text_encoder(y)
loss <- contrastive_alignment(z_img, z_txt)
update both encoders

at inference:
  use z_img for retrieval, zero-shot matching, or downstream probes
  optionally compare z_img against text prompt embeddings
```

3.4. Family IV: Multimodal generalist EO encoders

AnySat, Galileo, Prithvi, TerraFM, TerraMind, and DOFA represent a broader push toward modality-flexible or sensor-flexible Earth observation representation learning [15–17, 23–25]. These models are important because

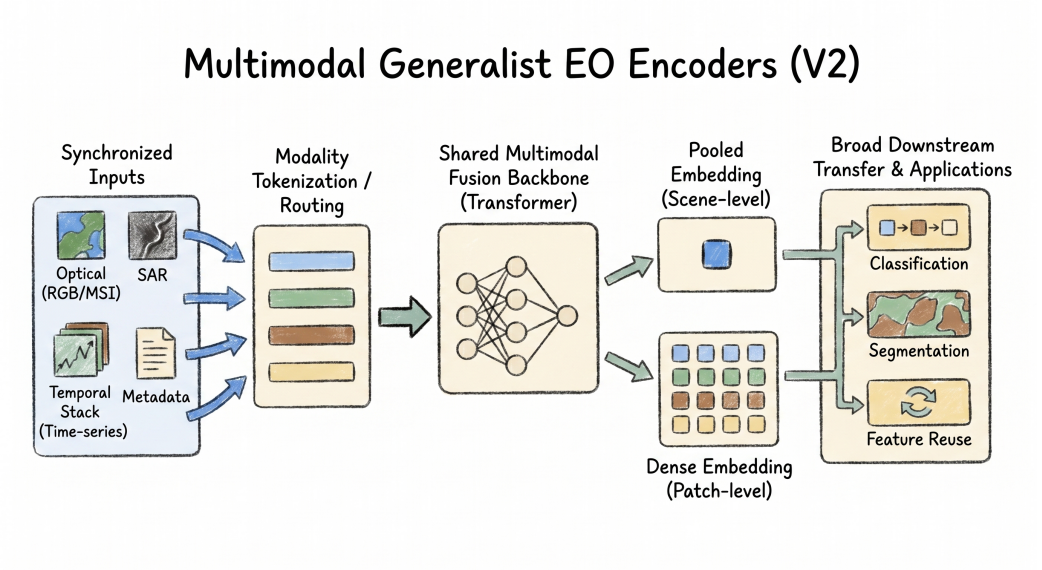

Figure 6: Unified architecture sketch for multimodal generalist EO encoders. Multiple sensor streams are tokenized, routed or aligned, fused by a shared backbone, and exported as pooled or dense representations for broad downstream transfer.

they move the field closer to a genuinely general EO representation space. Their distinguishing features include explicit handling of temporal stacks, wavelength metadata, modality routing, and cross-sensor alignment.

Architecture summary.. As Figure 6 summarizes, the defining goal of this family is not simply to process more inputs, but to learn a common representation space across sensors, scales, time, and metadata. Architecturally, that often means modality-specific tokenization combined with a shared transformer or fusion backbone. These models are closest to a true Earth observation foundation layer because they seek one latent space that remains useful under heterogeneous sensing conditions.

Pseudo-code template..

```
Input:
  modalities {x_1, x_2, ..., x_m}
  temporal or metadata context c

for each modality x_i:
    t_i <- modality_tokenizer_i(x_i, c)
```

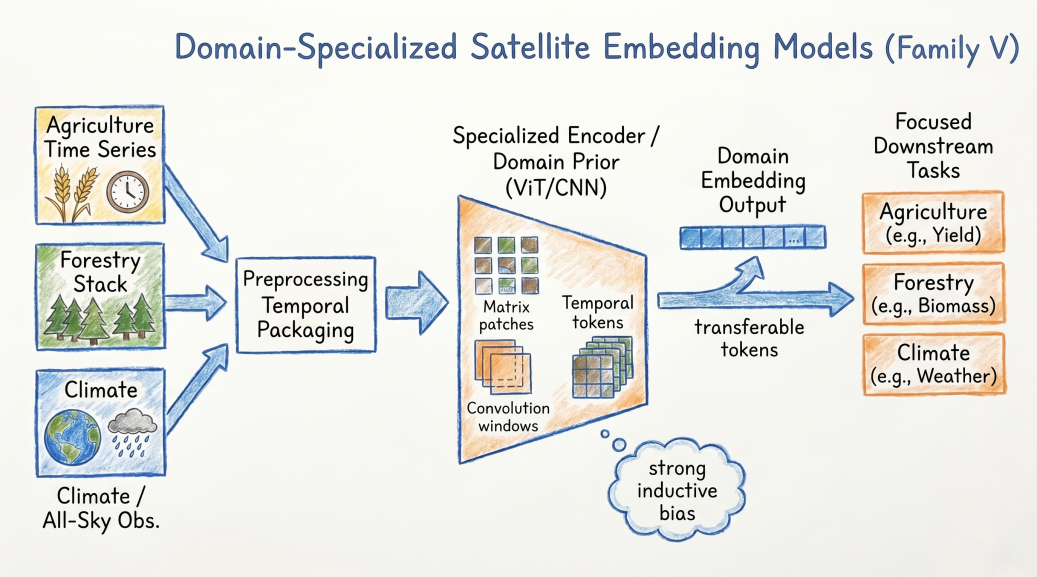

Figure 7: Unified architecture sketch for domain-specialized satellite embedding models. Domain-specific sensing pipelines and inductive biases are used to produce embeddings that are narrower in scope but often better matched to particular application regimes.

```
t_shared <- temporal_align_and_route({t_i}, c)
h <- multimodal_backbone(t_shared)
z_pool, z_grid <- readout(h)
optimize self-supervised or multimodal objective

return shared embeddings for cross-sensor downstream transfer
```

3.5. Family V: Domain-specialized embedding models

Not all useful satellite embeddings aim at maximal generality. AgriFM, FoMo, THOR, and SatVision show that domain-oriented models can remain highly valuable when their sensor assumptions and application context are well matched [26–29]. In a remote sensing review, these models should appear as a major family rather than as outliers, because they often reflect the real structure of EO practice: agriculture, forestry, biodiversity, atmosphere, climate, and societal monitoring all impose different representation demands.

Architecture summary.. As sketched in Figure 7, this family accepts a narrower operating domain in exchange for stronger inductive bias. Agricultural time series, forest monitoring stacks, climate-oriented inputs, or coarse all-sky observations are processed with task-aware temporal packaging, scale

handling, or specialized supervision. These models remind us that the best EO embedding is not always the most general one; in many real applications, domain fit matters more than universality.

Pseudo-code template..

```
Input:
  domain-specific sensor stream x
  domain labels or weak supervision y
  domain prior pi

x_tilde <- domain_preprocess(x, pi)
h <- specialized_encoder(x_tilde, pi)
z <- domain_embedding_head(h)
loss <- domain_objective(z, y, pi)
update model parameters

at deployment:
  reuse z for domain-focused mapping, monitoring, or regression
```

3.6. Cross-family comparison

After the family-level discussion, the review can return to a unified comparison table. This ordering is closer to the way remote sensing surveys are usually read: first understand the main branches of the field, then inspect the full inventory.

Table 1 turns the structured dossier into a paper-ready catalog. Unlike a compact leaderboard, it keeps the deployment type, sensing assumptions, temporal semantics, and pretraining regime visible, because these details strongly determine whether a model is suitable for retrieval, dense prediction, or operational mapping.

Table 1: Comprehensive model summary for the 19 canonical satellite embedding models currently exposed in `rs-embed`. The table emphasizes deployment-relevant details rather than only benchmark scores.

Model	Year	Venue	Type	Family	Backbone	Sensors / data	Resolution	Temporal semantics	Emb. / output	Pretraining signal
tessera	2026	CVPR	precomputed	Precomputed temporal embedding field	field model over surface spectra embeddings	surface spectra product	10 m precomputed embedding tiles	annual lookup over product years	128; pooled, grid	embedding field regression / product training
gse	2025	arXiv	precomputed	Precomputed annual embedding product	embedding field model	Google Satellite Embedding annual product	10 m annual embedding product	strict yearly product	64; pooled, grid	global embedding field learning from sparse labels
copernicus	2025	ICCV	precomputed	Precomputed foundation map	Copernicus foundation model product	Copernicus product stack	0.25° precomputed grid	static in current adapter (2021 only)	768; pooled, grid	foundation model pretraining followed by product distillation
remoteclip	2024	IEEE TGRS	on-the-fly	Vision-language satellite embedding	CLIP / ViT-B-32	Sentinel-2 RGB, remote sensing captions, UAV imagery in pretraining	10 m; Sentinel-2 RGB	single composited observation window at inference	768; pooled, grid	contrastive image-text alignment (InfoNCE)
satmae	2022	NeurIPS	on-the-fly	Masked autoencoder for temporal or multispectral EO	ViT-MAE	Sentinel-2 RGB or multispectral/time-series variants in original paper	10 m; Sentinel-2 RGB	explicit temporal embeddings in the original paper; rs-embed adapter currently uses RGB composite path	1024; pooled, grid	masked autoencoding with temporal/spectral positional encoding
satmaepp	2024	CVPR	on-the-fly	Improved masked autoencoder for EO	ViT-L / SatMAE++	Sentinel-2 RGB in adapter, multispectral Sentinel-2 in paper	10 m; Sentinel-2 RGB	single composited observation window in adapter	1024; pooled, grid	revised MAE pretraining for multispectral satellite imagery
satmaepp_s2_10b	2024	CVPR	on-the-fly	Grouped-channel multispectral masked autoencoder	ViT-L / grouped-channel SatMAE++	Sentinel-2 SR 10-band	10 m; Sentinel-2 SR 10-band input	single composited observation window in adapter	1024; pooled, grid	grouped-channel masked autoencoding
scalemae	2023	ICCV	on-the-fly	Scale-aware masked autoencoder	ViT-L / MAE	Sentinel-2 RGB in adapter, multiscale EO imagery in paper	10 m; Sentinel-2 RGB, plus explicit semantic scale input	single composited observation window	1024; pooled, grid	masked autoencoding with explicit resolution conditioning

Table 1: Comprehensive model summary for the canonical `rs-embed` model set (continued).

Model	Year	Venue	Type	Family	Backbone	Sensors / data	Resolution	Temporal semantics	Emb. / output	Pretraining signal
anysat	2025	CVPR	on-the-fly	Generalist multi-resolution multi-modal EO encoder	versatile JEPA-style EO encoder	Sentinel-2, Sentinel-1, aerial/VHR and other modalities in original paper	10 m Sentinel-2 time-series input; default per-frame resize 24 px	multi-frame optical sequence with date tokens	768; pooled, grid	self-supervised representation learning across many configurations
galileo	2025	ICML	on-the-fly	Global-local multimodal time-series encoder	transformer with global/local branches	Sentinel-2 time series, multiple remote sensing modalities in original work	10 m Sentinel-2 time-series input; default frame size 64 px, patch size 8	explicit month tokens and frame masks	128; pooled, grid	self-supervised multimodal representation learning
wildsat	2025	ICCV	on-the-fly	Remote sensing representation learning from weak labels	ViT-B-16	Sentinel-2 RGB, wildlife observations as supervision	10 m; Sentinel-2 RGB	single composited optical patch	256; pooled, grid	supervised / weakly supervised representation learning from wildlife observations
prithvi	2023	arXiv	on-the-fly	Generalist geospatial foundation model	ViT / masked autoencoder lineage	HLS / Sentinel-Landsat style 6-band optical imagery	30 m in current adapter; Sentinel-2 6-band input	explicit temporal coordinates in adapter and paper family	768; pooled, grid	self-supervised geospatial pretraining
terrafm	2026	ICLR	on-the-fly	Unified multisensor foundation model	multisensor transformer	Sentinel-2, Sentinel-1	10 m for both S2 and S1 paths; image resized to 224 px	single observation window in current adapter; paper focuses on multisensor unification	768; pooled, grid	scalable unified multisensor pretraining
terramind	2025	ICCV	on-the-fly	Generative multimodal EO foundation model	large-scale generative multimodal transformer	Sentinel-2 in adapter, wider multimodal EO stack in paper	10 m; Sentinel-2 SR 12-band input; image resized to 224 px	single composited optical path in adapter	384; pooled, grid	large-scale generative multimodal learning
dofa	2024	arXiv	on-the-fly	Wavelength-aware multimodal foundation model	transformer with neural plasticity / dynamic wavelength handling	multispectral and hyperspectral style inputs, Sentinel-2 in adapter	10 m for S2 path; fixed resize to 224 px	single observation window in adapter	768; pooled, grid	self-supervised multimodal EO foundation modeling

Table 1: Comprehensive model summary for the canonical `rs-embed` model set (continued).

Model	Year	Venue	Type	Family	Backbone	Sensors / data	Resolution	Temporal semantics	Emb. / output	Pretraining signal
fomo	2025	AAAI	on-the-fly	Forest-oriented multimodal and multiscale foundation model	multimodal transformer / representation learner	Sentinel-2 SR in adapter, multiple scales and tasks in original work	10 m; Sentinel-2 SR 12-band input; default image size 64 px	single optical composite in adapter	768; pooled, grid	multi-task forest monitoring pretraining
thor	2026	arXiv	on-the-fly	Versatile EO foundation model for climate and society	versatile transformer	Sentinel-2 SR 10-band	10 m; Sentinel-2 SR 10-band input; default image size 288 px	single optical composite in adapter	768; pooled, grid	foundation pretraining for climate and society applications
agrifm	2026	Remote Sensing of Environment	on-the-fly	Agriculture-specific multi-source temporal foundation model	Video Swin Transformer	Sentinel-2 in adapter, Sentinel-2, Landsat-8/9, MODIS in original paper	10 m Sentinel-2 time-series input; default image size 224 px with fixed T-frame packaging	fixed-length multi-frame temporal stack	1024; pooled, grid	supervised land-cover fraction pretraining with EMA teacher
satvision	2024	arXiv	on-the-fly	Coarse-resolution all-sky foundation model	SwinV2-style encoder	MODIS 14-band TOA	1000 m; 14-channel TOA input	single coarse-resolution observation window in adapter	4096; pooled, grid	foundation pretraining on all-sky MODIS TOA data

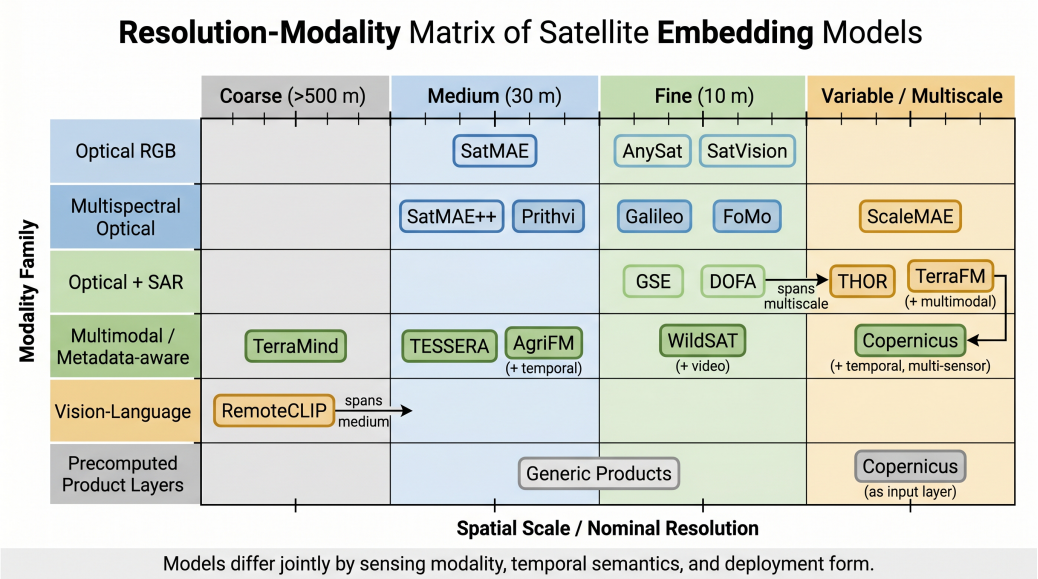

Figure 8: Resolution-modality matrix for current satellite embedding models. The same model family can occupy very different parts of the sensing space, from coarse-resolution all-sky imagery to high-resolution optical-SAR or multimodal temporal embeddings.

Three contrasts recur across families. First, precomputed layers prioritize access and coverage, while on-the-fly encoders prioritize flexibility. Second, multimodal and time-aware systems attempt to absorb sensor heterogeneity at training time, whereas narrower families often compensate with stronger specialization and simpler deployment. Third, vision-language models add open-vocabulary semantics that are mostly absent from pure masked reconstruction pipelines. These contrasts matter more for a review paper than a single benchmark leaderboard, because they explain why different families remain competitive under different downstream conditions.

Figure 8 closes this section by summarizing the sensing space covered by current models. In a remote sensing context, this figure is often more informative than a single ranking table because it makes sensor assumptions and scale mismatch immediately visible.

4. Data Resources, Application Space, and Evaluation Logic

Recent remote sensing review articles in RSE, TGRS, and ISPRS tend to avoid treating methods, datasets, and applications as isolated lists. Instead,

they first describe the sensing and data regime, then organize methodological families around the downstream questions that remote sensing users actually ask, and finally return to limitations, scale effects, and evaluation practice [1, 30–35]. This organization is especially appropriate for satellite embeddings because an embedding is not a complete solution by itself. It is an intermediate representation whose usefulness depends on the sensor stream from which it was learned, the spatial and temporal scale at which it is exposed, and the type of downstream evidence that a user wants to recover. A pooled vector can be excellent for tile classification but insufficient for shoreline delineation; a dense feature grid can support segmentation but may be expensive or unavailable for some products; an annual precomputed layer can be ideal for wide-area screening but poorly matched to event-specific monitoring. The application section therefore has to do more than enumerate tasks. It must explain how the embedding form constrains the mapping problem.

The first organizing dimension is the data regime. Most current satellite embeddings are produced from one of four recurring sources: medium-resolution optical archives such as Sentinel-2 and Landsat, optical-SAR combinations centered on Sentinel-1 and Sentinel-2, broader multimodal stacks that add elevation, weather, labels, text, or metadata, and precomputed embedding products that have already collapsed a large archive into a queryable feature layer. These regimes create different forms of transfer. Optical-only models usually retain strong spectral and spatial cues for land-cover mapping, but they may fail under cloud, season, or sensor changes if temporal handling is weak. Optical-SAR and multimodal models try to absorb those changes during representation learning, but their practical value depends on whether all required inputs are available in the target region and period. Precomputed products shift the problem again: they reduce inference cost and make wide-area sampling simple, yet they also fix the upstream temporal summary, native scale, and production assumptions. This is why the same model family can behave very differently when evaluated at 10 m, 30 m, 500 m, 1 km, or 0.25° resolution. In an embedding-centered review, native scale is not a footnote; it is part of the representation.

The second organizing dimension is the downstream target. Classification and mapping remain the most common entry point because they are compatible with almost every embedding family. A single pooled vector per tile is often enough to support land-cover labels, crop categories, forest condition classes, urban typologies, or simple ecological strata. This makes

classification a useful baseline, but it is also an incomplete test: a model can separate dominant classes while losing continuous mixture information or local boundary structure. Regression tasks address that gap by asking whether the embedding preserves smoothly varying quantities such as built-up fraction, vegetation fraction, biomass proxies, canopy height, crop-yield indicators, or environmental indices. Dense prediction tasks push further by asking whether the representation still contains spatially localized information after tokenization, pooling, product resampling, or temporal summarization. Water extraction, land-cover segmentation, flood mapping, and mask reconstruction are therefore not merely additional applications; they probe whether the embedding is a spatial representation rather than only a semantic descriptor. Finally, vision-language and cross-modal embeddings introduce retrieval and open-vocabulary search as a distinct mode of use. These tasks are promising, but they should be interpreted separately from supervised mapping because they measure semantic alignment and promptability rather than only geographic fidelity.

The third organizing dimension is operational fit. Remote sensing users rarely choose an embedding only because it has the highest number in a table. They also need to know whether the representation can be generated for the desired sensor, season, and region; whether it exposes pooled or dense outputs; whether it can be sampled as a product or requires GPU inference; whether runtime and memory scale with area; and whether the temporal meaning of the output is annual, seasonal, monthly, or scene-specific. Recent foundation-model surveys have emphasized the same concern from a broader model perspective, but embedding selection makes it even sharper: two systems can both be called foundation models while exposing very different reusable objects [1–3, 35]. The review therefore treats applications as representation tests. Classification tests semantic separability, regression tests continuous structure, binary extraction tests operational thresholdability, segmentation tests local spatial separability, and retrieval tests cross-modal alignment. This evaluation logic leads directly to the compact benchmark in the next section.

5. A Compact Wuhan Benchmark for Satellite Embeddings

The empirical component of this review is intentionally modest in geographic scope but strict in comparison logic. Rather than assembling unrelated benchmark numbers from model papers, we evaluate all 19 public

models on one high-resolution Wuhan ROI covering the East Lake–Tangxun Lake corridor. The region is useful for a first controlled comparison because it contains a compact mixture of open water, dense urban fabric, vegetation, cropland, and mixed transition zones. That mixture is large enough to expose scale and representation differences, but small enough to make repeated extraction, cache checking, and visual inspection feasible. This follows the spirit of benchmark-oriented remote sensing reviews, where a local protocol is not presented as a substitute for global validation, but as a controlled lens for understanding how methods behave under shared data, labels, and evaluation rules [20, 34, 36].

All benchmark tasks use the same 500 m tile grid, the same train/validation/test split, and lightweight heads fitted on frozen embeddings. The protocol deliberately avoids end-to-end fine-tuning because the goal is to compare the information already present in each reusable representation. On-the-fly encoders are run or cached over the same Wuhan window, while precomputed products are sampled at the nearest compatible temporal layer and resampled only as needed for the shared tile grid. This design makes the comparison fairer than reading model-paper leaderboards, but it also keeps the interpretation honest: the results describe local transfer under one urban-lake landscape, not universal model superiority. The benchmark is therefore best read as a diagnostic complement to the literature review. It asks which embeddings preserve class separability, continuous land-cover mixture, water/non-water thresholdability, and dense class structure when the geography, labels, and probe complexity are held fixed.

the initial 15-tile pilot: it keeps the same region and label semantics, but tests whether the observed model differences remain visible across a larger, Figure 9 summarizes the benchmark pipeline. The executed version uses the current two-by-two Wuhan window, which expands the original visual sanity case to four adjacent Sentinel-2 blocks and 567 valid 500 m tiles. Labels are derived from ESA WorldCover 2021 and JRC Global Surface Water, then converted into four related evaluation views: dominant land-cover classification, built-up/vegetation/cropland/water fraction regression, binary water extraction, and dense multi-class threshold segmentation. These tasks are deliberately related rather than independent. The same tile that is easy to classify as water may still be difficult near a mixed shoreline; the same embedding that ranks vegetation fraction well may still blur cropland boundaries; and the same product that looks coherent in a map may fail when its native grid is too coarse for 500 m probing. Using related tasks over one ROI there-

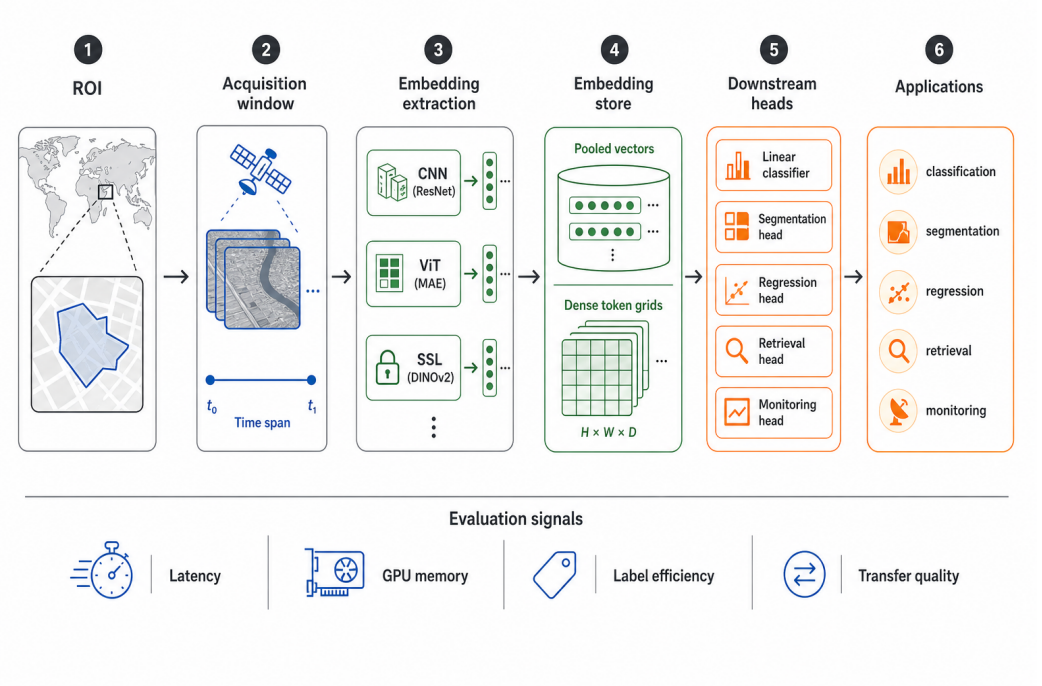

Figure 9: Application-oriented benchmark pipeline. A shared region of interest is converted into a unified embedding extraction workflow, lightweight probe heads, and downstream evaluation targets spanning classification, segmentation, regression, and retrieval.

fore makes the benchmark more diagnostic than a collection of disconnected scores.

Figure 10 provides the visual acceptance case for this expanded benchmark before any downstream probe is fitted. The upper-left reference panel shows the original 2x Wuhan window, while the remaining panels show the corresponding model-specific embedding maps for the 19 public models. The comparison is intentionally qualitative: it checks whether the exported embeddings preserve a recognizable spatial organization over the same geographic footprint. Several models recover the lake corridor and surrounding urban-vegetation contrast as coherent regions, whereas coarser or less spatially matched representations appear flatter, blockier, or less locally structured. This figure therefore establishes that the downstream classification and regression tasks are being run on a common region where the models already expose visibly different spatial behavior.

The qualitative overview in Figure 10 is an important first check before

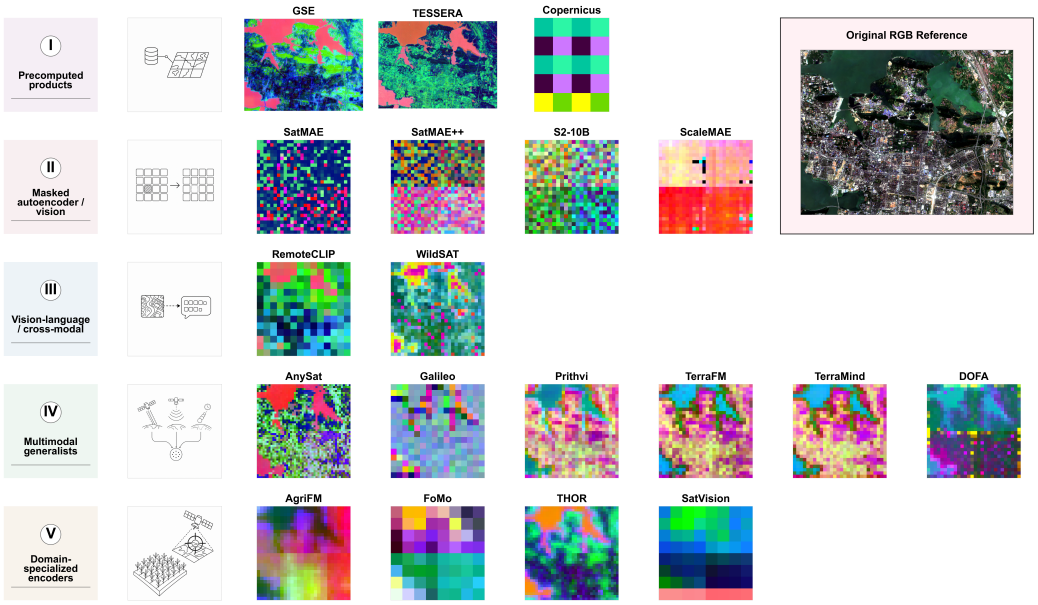

Figure 10: Original imagery and public-model embedding maps for the two-by-two Wuhan benchmark window. The reference image anchors the shared geographic footprint, and the remaining panels show how the 19 public embeddings organize the same region before task-specific probes are fitted.

any downstream probe is fitted. The upper-left panel anchors the shared geography, and the remaining panels show how each model organizes the same region in embedding space. Several models recover the lake corridor and surrounding urban-vegetation contrast as coherent structures, while coarser or less spatially matched representations appear flatter, blockier, or less locally organized. This visual step is not a substitute for metrics, but it prevents the benchmark from becoming a detached leaderboard: it confirms that the downstream tasks are comparing embeddings over a common footprint where model families already expose visibly different spatial behavior.

For tile-level land-cover classification, the frozen-embedding linear probe shows a clear leading group (Figure 11). GSE obtains the strongest result with 0.890 test macro-F1, 0.971 balanced accuracy, and 0.956 overall accuracy. AnySat and TESSERA form the next tier, with macro-F1 scores of 0.836 and 0.830, respectively. A broader middle group including THOR, TerraMind, Prithvi, TerraFM, WildSat, DOFA, and AgriFM reaches useful overall accuracy, but lower macro-F1 indicates that minority or confusable

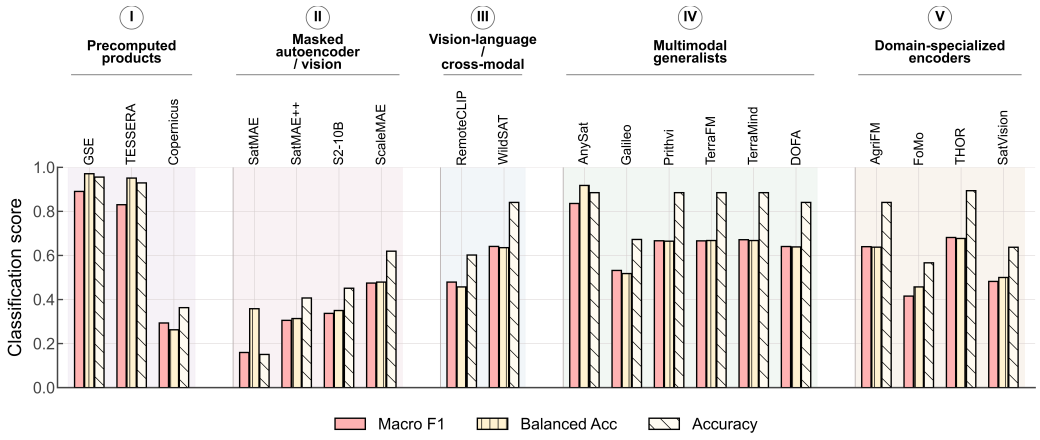

Figure 11: Tile-level land-cover classification on the two-by-two Wuhan benchmark window. Bars report public-model test performance from frozen embeddings and a lightweight linear probe over the shared 500 m tile split.

classes remain harder than the dominant landscape categories. The weakest results come from several RGB- or scale-mismatched checkpoints and the coarse Copernicus product, which confirms that deployment scale and input compatibility are not secondary details for local 500 m mapping. The spatial prediction maps in Figure 12 add the geographic diagnosis behind the scores. The best models preserve the main water, green, and built-up structure of the corridor, while weaker models show either over-smoothed regions or fragmented transitions. In this respect, classification acts as the broadest representation test: it asks whether a frozen embedding contains enough semantic information for a simple probe to recover the dominant landscape pattern.

The spatial prediction maps in Figure 12 adds an important diagnostic that a single leaderboard cannot provide. The best models preserve the main water, green, and built-up structure of the corridor, while weaker models show either over-smoothed regions or fragmented class transitions. These maps are useful for the survey because they expose whether a model's score reflects coherent geographic behavior or only aggregate class counts. In particular, the maps make the scale mismatch of coarser products visually apparent, while the leading precomputed and multimodal embeddings produce more stable spatial patterns over the same tile lattice.

The fraction-regression task evaluates a complementary property: whether

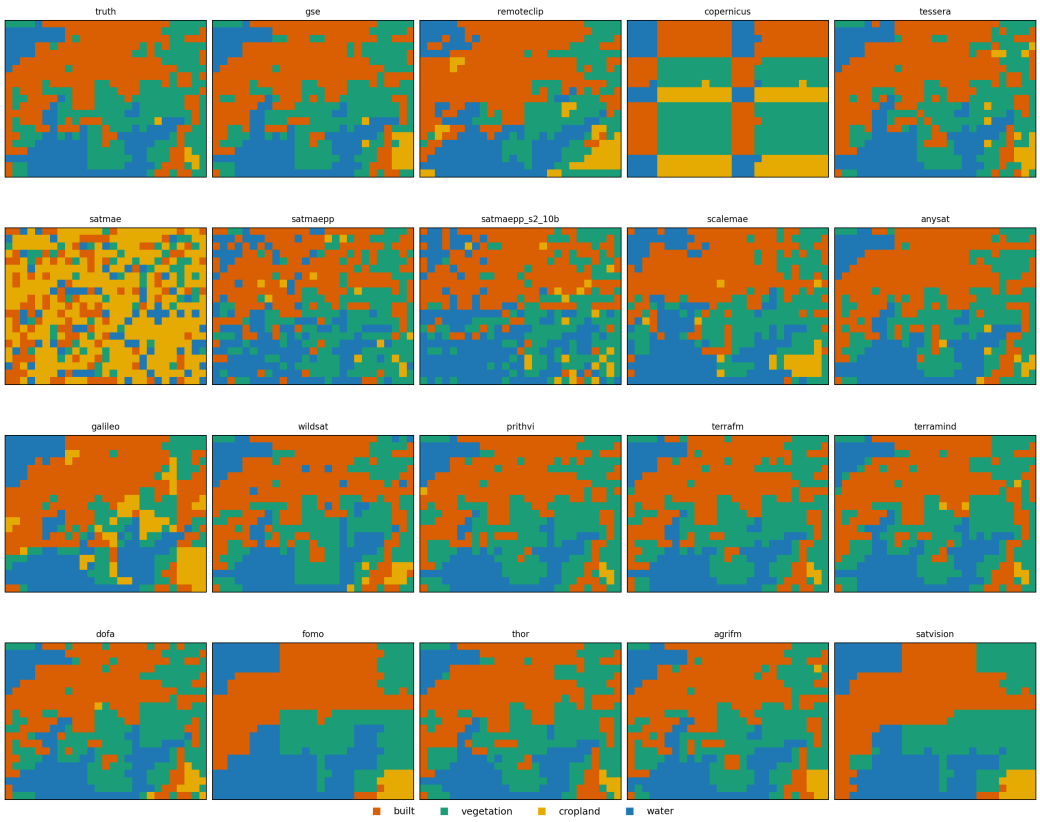

Figure 12: Per-model classification maps for the two-by-two Wuhan benchmark window. Each panel uses the same 500 m tile grid and split-derived probe, allowing spatial errors and over-smoothing to be compared across all 19 public models.

the embedding preserves smoothly varying land-cover composition rather than only a dominant class label. Using ridge probes over built-up, vegetation, cropland, and water fractions, GSE again ranks first with a mean test Spearman correlation of 0.881 (Figure 13). TESSERA and THOR follow closely at 0.866 and 0.852, while DOFA, TerraMind, AgriFM, Prithvi, AnySat, and TerraFM remain in a competitive middle band. The strongest models are especially consistent for built-up and vegetation fractions, where several models exceed 0.90 Spearman correlation. Cropland and water are harder in this urban-lake corridor, producing wider differences across models and making the mean score a useful summary of robustness across target variables. Figure 14 gives the point-level view behind the ranking. In the

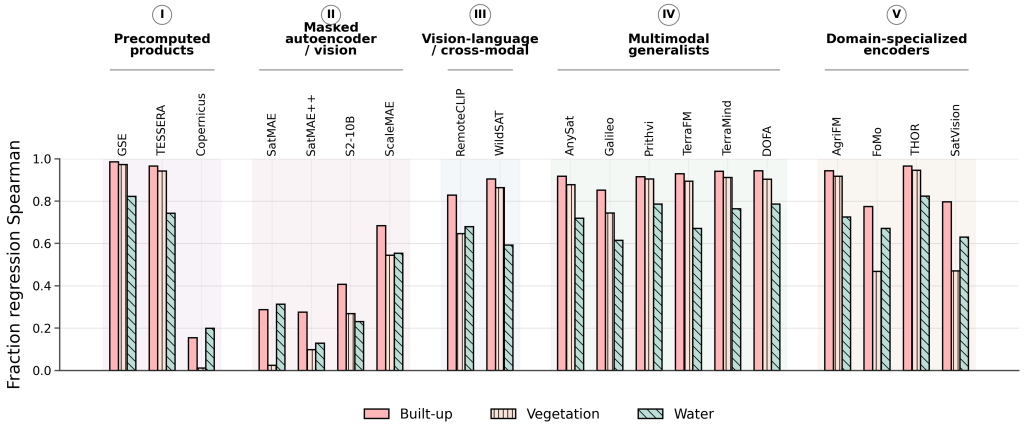

Figure 13: Fraction-regression performance on the two-by-two Wuhan benchmark window. Bars summarize test Spearman correlation across built-up, vegetation, cropland, and water fraction targets using cached public-model embeddings and ridge regression probes.

strongest panels, the cloud of points follows the one-to-one diagonal for built-up and vegetation fractions, indicating that the probe is not only ordering tiles correctly but also recovering approximate sub-tile proportions. The middle-tier models retain the main monotonic trend but show broader vertical spread, especially for cropland and water. The weakest models show compressed predictions or diffuse point clouds, meaning that their embeddings contain less recoverable information about continuous land-cover mixture in this local setting.

Figure 14 gives the point-level view behind the regression ranking. In the strongest panels, the cloud of points follows the one-to-one diagonal for built-up and vegetation fractions, indicating that the probe is not only ordering tiles correctly but also recovering approximate sub-tile proportions. GSE, TESSERA, and THOR show the tightest alignment across targets, which is consistent with their leading mean Spearman scores. The middle-tier models retain the main monotonic trend but show broader vertical spread, especially for cropland and water. The weakest models show compressed predictions or diffuse point clouds, meaning that their embeddings contain less recoverable information about continuous land-cover mixture in this local setting. Read together with Figure 13, the scatter plot clarifies that high regression performance corresponds to both rank consistency and visually calibrated fraction

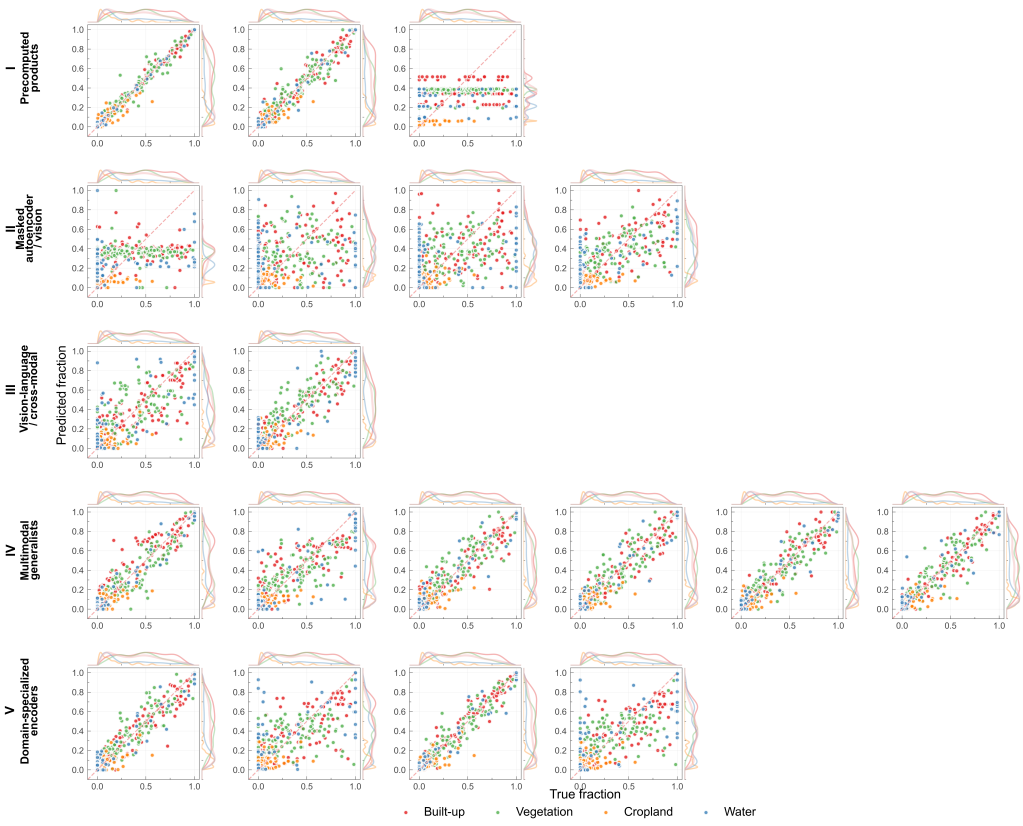

Figure 14: Predicted versus reference fraction-regression scatter plots for all public models on the two-by-two Wuhan benchmark. The panels diagnose whether continuous land-cover proportions are preserved in the frozen embeddings beyond dominant-class classification.

estimates, rather than to a single averaged leaderboard value.

Water extraction isolates a more operational decision. A tile is treated as water when at least half of its area is covered by the JRC-derived binary water mask, yielding 185 positive tiles out of 567 in the two-by-two Wuhan window. Unlike fraction regression, this task asks whether a frozen embedding can support a threshold-like water/non-water decision with a lightweight linear probe. Figure 15 shows that DOFA is the strongest model on this binary extraction task, reaching 0.895 test IoU and 0.944 F1. THOR, TerraMind, TerraFM, TESSERA, GSE, AnySat, Prithvi, and AgriFM form a strong middle-to-high group, all above 0.75 IoU. The map panels in Figure 16 provide the spatial counterpart to the leaderboard: high-performing models

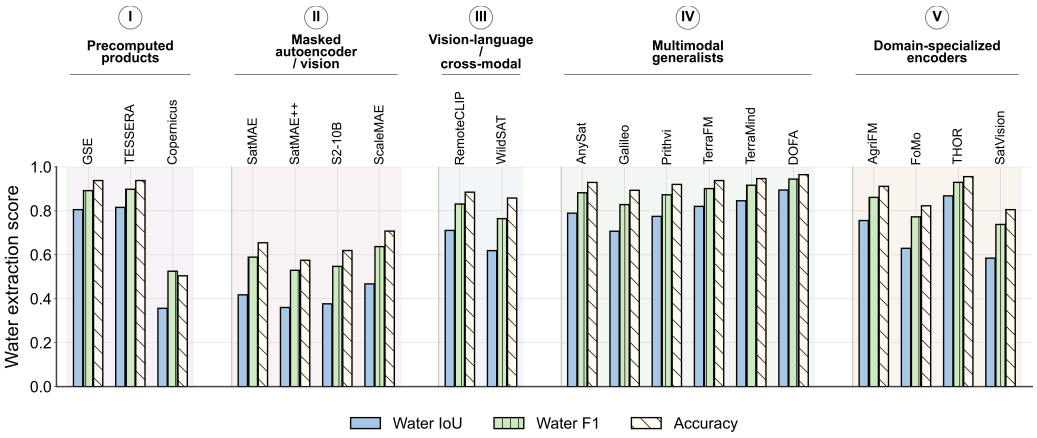

Figure 15: Water extraction performance on the two-by-two Wuhan benchmark window. Bars report test IoU, F1, and accuracy for frozen public-model embeddings with a CUDA-trained linear binary probe over the shared 500 m tile split.

recover the continuous lake corridor and suppress most built-up or vegetated non-water tiles, while weaker models either over-predict water along mixed boundaries or miss smaller water-adjacent tiles. This task is useful because it sits between coarse classification and dense segmentation. It is operationally meaningful, yet still compatible with pooled tile embeddings for all public models.

The map panels in Figure 16 provide the spatial counterpart to the water-extraction leaderboard. High-performing models recover the continuous lake corridor and suppress most built-up or vegetated non-water tiles, while weaker models either over-predict water along mixed boundaries or miss smaller water-adjacent tiles. This visual diagnostic is important because binary IoU alone cannot distinguish a coherent shoreline error from scattered false positives. Together, the metric and map views show that water extraction is a useful intermediate task between coarse tile classification and dense segmentation: it is operationally meaningful, but still compatible with pooled tile embeddings for all 19 public models.

The final task moves from binary water extraction to dense multi-class segmentation. Here the target is the four-class WorldCover-derived mask used throughout the benchmark: built-up, vegetation, cropland, and water. For each model, class prototypes are estimated from prompted pixels in the dense embedding grid, class-specific thresholds are calibrated on the vali-

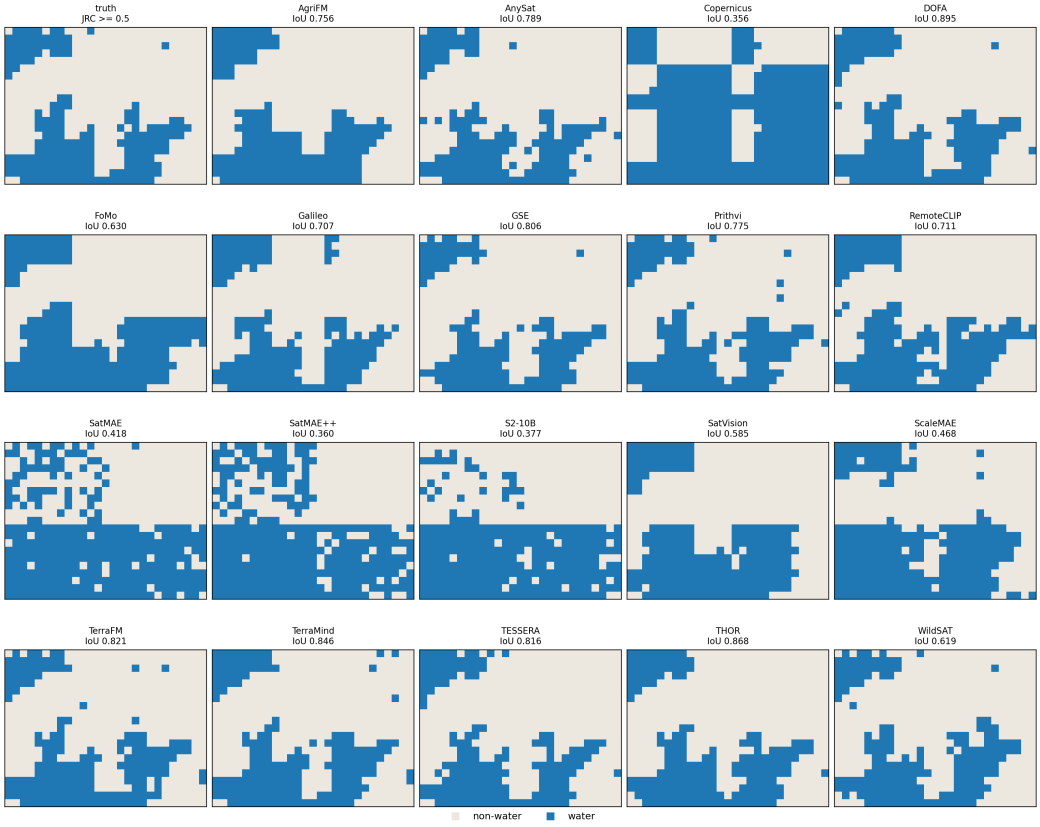

Figure 16: JRC water truth and public-model water-extraction maps for the two-by-two Wuhan benchmark window. Each model predicts water/non-water labels on the same 500 m tile grid, making shoreline coherence and false-positive patterns directly comparable across all 19 public models.

dation split, and the resulting mask is evaluated on the held-out test split. This is closer to a SAM-style use of embeddings than the preceding probe tasks: the model is not trained end-to-end for segmentation, but its dense representation is queried with class prompts and converted into a mask by thresholding. Figure 17 shows that GSE is the clear leader for this dense multi-class setting, reaching 0.615 test mIoU, 0.700 macro-F1, and 0.833 accuracy. TESSERA ranks second with 0.503 mIoU, followed by AnySat and AgriFM. The class-wise scores reveal an important asymmetry: water is recovered well by the leading models, while cropland remains difficult because it occupies a small and spatially mixed portion of the two-by-two window.

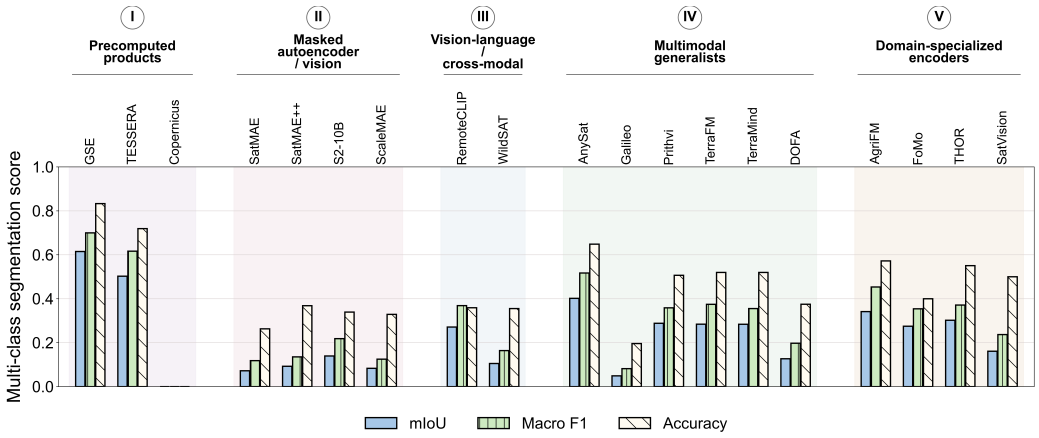

Figure 17: SAM-like multi-class threshold segmentation on the two-by-two Wuhan benchmark window. Bars report test mIoU, macro-F1, and accuracy for built-up, vegetation, cropland, and water masks derived from dense public embeddings with validation-calibrated class thresholds.

Figure 18 makes this asymmetry visible. GSE and TESSERA preserve the strongest correspondence to the WorldCover reference, especially for the lake and larger built-up or vegetated zones. AnySat and AgriFM recover the broad water and green structure but lose more detail at class boundaries. Several lower-ranked models collapse toward one or two dominant classes, showing that their dense maps contain less separable class information under this prompt-threshold protocol.

The maps in Figure 18 make these differences visible. GSE and TESSERA preserve the strongest correspondence to the WorldCover reference, especially for the lake and larger built-up or vegetated zones. AnySat and AgriFM recover the broad water and green structure but lose more detail at class boundaries. Several lower-ranked models collapse toward one or two dominant classes, showing that their dense maps contain less separable class information under this prompt-threshold protocol. Copernicus is again a scale-mismatch failure case: its native product grid is too coarse for a local dense segmentation benchmark of this size.

Across the four tasks, three conclusions are more important than the exact ordering of every model. First, productized and multimodal embeddings are highly competitive in this local setting. GSE is the strongest or near-strongest model in classification, fraction regression, and dense segmentation, while TESSERA, THOR, DOFA, TerraMind, AnySat, and AgriFM recur in

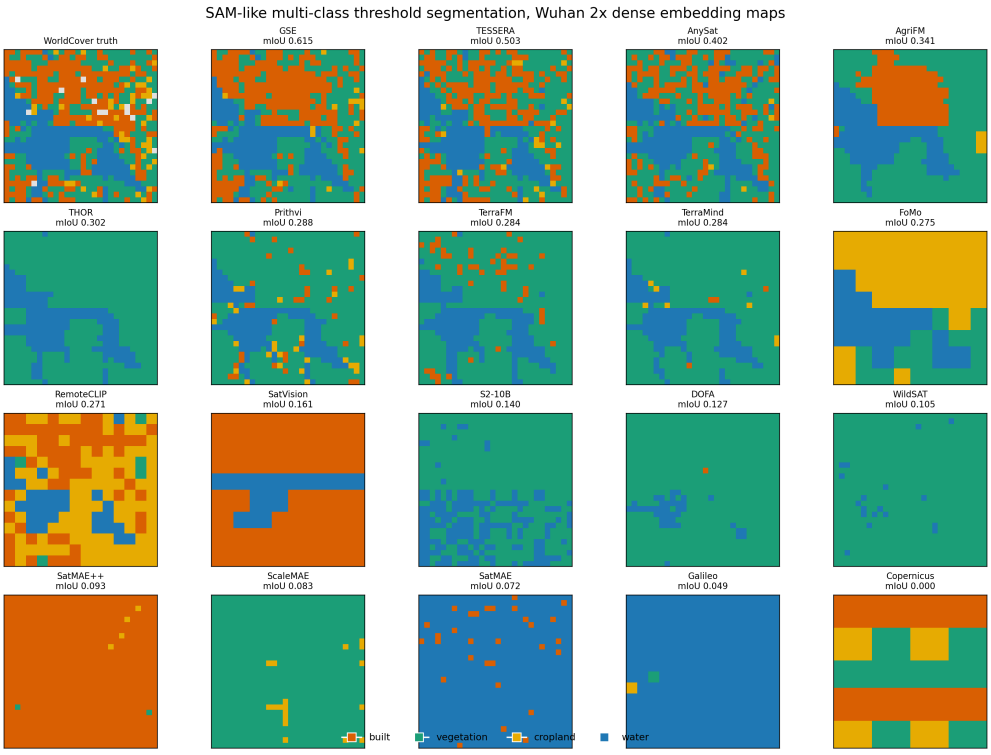

Figure 18: WorldCover truth and public-model multi-class threshold segmentation maps for the two-by-two Wuhan benchmark window. Panels use the same four classes—built-up, vegetation, cropland, and water—so class collapse, boundary errors, and scale mismatch can be visually compared across all 19 public models.

the upper or middle tiers depending on the task. Second, the benchmark repeatedly exposes scale mismatch. Coarse products or checkpoints whose input assumptions are poorly aligned with a 500 m local Sentinel-2 window can fail even when they are useful at their native scale. This does not make those models weak in general; it shows that embedding evaluation must respect the spatial unit at which the representation is produced. Third, no single metric captures all useful behavior. Classification highlights dominant semantic separability, regression highlights continuous mixture structure, water extraction highlights operational thresholdability, and dense segmentation highlights local spatial separability. Read together, the Wuhan benchmark supports the main claim of the review: satellite embeddings should be compared as reusable geospatial representations, not only as model names or pretraining recipes.

6. Open Challenges and Future Directions

The review and Wuhan benchmark point to several challenges that are now becoming central for satellite embeddings. The first is temporal ambiguity. Many current systems use the same word, embedding, for annual products, short seasonal composites, single-date observations, and multi-step time series. These objects can all be useful, but they do not preserve the same temporal information. A representation that averages a year of observations may be stable for land-cover mapping but poorly suited to flood response or phenology-sensitive agriculture; a temporal encoder may preserve seasonal dynamics but require inputs that are difficult to obtain in cloudy or data-sparse regions; a precomputed product may be easy to sample but locked to the upstream production calendar. Future papers should therefore report not only the sensor and spatial resolution of an embedding, but also its temporal support, compositing rule, update frequency, and intended interpretation. This would make model selection more transparent and would prevent annual products, scene encoders, and temporal sequence models from being compared as if they were the same representation.

The second challenge is scale mismatch. Remote sensing reviews have long emphasized that spatial, spectral, and temporal resolution determine what can be observed, but foundation-model discussions sometimes hide this fact behind architecture names. The Wuhan benchmark makes the issue concrete: embeddings produced at 10 m, 30 m, 500 m, 1 km, or 0.25° are not interchangeable, and resampling cannot create local information that was never present in the native representation. This is especially important for precomputed products because their convenience can encourage users to sample them outside the scale at which they are meaningful. A stronger evaluation culture would report native support, resampling choices, and target grid size together with accuracy. It would also include visual diagnostics, because map coherence often reveals scale failure before a single aggregate metric does.

The third challenge is the comparison between products and checkpoints. Precomputed embedding fields optimize access, coverage, and repeatability; on-the-fly encoders optimize flexibility, temporal control, and adaptation to new inputs. Both are legitimate satellite embedding regimes, but they should not be evaluated only by the same predictive score. Product models should be credited for low inference burden, stable large-area sampling, and reproducible feature layers. Checkpoint models should be credited for

sensor-specific control, temporal customization, dense readout options, and the ability to adapt to new data streams. Future benchmarks should therefore pair quality metrics with deployment metrics such as extraction latency, GPU memory, missing-data behavior, storage footprint, and product availability. This is not an engineering afterthought. For Earth observation, these constraints often decide whether a representation can be used at continental scale or in repeated monitoring.

The fourth challenge is application realism. Standard remote sensing datasets remain valuable, but satellite embeddings are increasingly used in settings that do not look like benchmark leaderboards: sparse labels, mixed pixels, shifting seasons, changing sensors, region transfer, and continuous environmental quantities. The Wuhan benchmark is only a first step, yet it shows why related task families are useful. Classification, regression, water extraction, and segmentation expose different failure modes over the same region. Future work should extend this logic to larger and more diverse ROIs, cross-year splits, few-label protocols, and physically meaningful regression targets such as canopy height, biomass, crop condition, surface water dynamics, and urban intensity. The field also needs clearer reporting of negative results. A model that fails because of scale mismatch, unavailable inputs, or temporal misalignment teaches a different lesson from a model that fails because its representation is weak.

Finally, satellite embeddings need more standardized reporting. A useful model card for this area should include the pretraining data regime, sensor assumptions, native spatial and temporal support, output forms, embedding dimensionality, dense-readout availability, licensing or product access, and recommended downstream usage. Recent systems such as Prithvi-EO-2.0 and FlexiMo show that the field is continuing to expand toward more flexible multitemporal and multimodal representations [37, 38]. As that expansion continues, the review problem will become less about whether a model is a foundation model and more about whether its embedding is the right geospatial object for a given task. The next generation of surveys should therefore combine taxonomy, evidence, and reporting standards rather than treating model inventories as sufficient.

7. Conclusion

Satellite embeddings are becoming a practical abstraction layer for Earth observation. They connect large archives, foundation-model training, pre-

computed products, and lightweight downstream analysis, but the literature still tends to describe them indirectly through model families or benchmark datasets. This review argues for a more direct framing: the reusable representation itself should be the unit of organization. From that perspective, precomputed products, masked autoencoders, vision-language encoders, multimodal generalists, and domain-specialized models can be compared as different ways of producing transferable geospatial features under different sensing assumptions.

The main contribution of the review is therefore twofold. First, it provides an embedding-centered taxonomy and model dossier for 19 representative public models, making sensor support, temporal semantics, output form, dimensionality, and deployment mode visible alongside architecture and pretraining objective. Second, it links that taxonomy to a compact Wuhan benchmark that evaluates frozen embeddings under shared geographic, label, and probe conditions. The results show that model choice depends on the target property being tested: semantic separability, continuous land-cover mixture, water thresholdability, and dense spatial separability emphasize different strengths and weaknesses. They also show that scale mismatch is not a minor implementation detail, but a central factor in whether an embedding is meaningful for local mapping.

The broader lesson is that satellite embeddings should be selected and evaluated as geospatial representations, not only as checkpoints. A useful review must therefore connect literature synthesis with data regimes, application requirements, operational constraints, and empirical diagnostics. The current paper is a step in that direction: it keeps the broad survey structure of recent remote sensing reviews, but adds an embedding-specific benchmark lens that makes representation behavior visible in one controlled ROI. Future extensions should scale this evidence across regions, years, and physically grounded regression targets while preserving the same principle: compare embeddings in the form practitioners actually use them.

CRediT authorship contribution statement

Longhao Wang: Conceptualization, Methodology, Software, Validation, Formal analysis, Investigation, Data curation, Writing–original draft, Writing–review and editing, Visualization.

Declaration of competing interest

The author declares that there are no known competing financial interests or personal relationships that could have appeared to influence the work reported in this paper.

Data availability

The benchmark uses publicly available Earth observation data products and public model artifacts described in the manuscript. Code and derived experiment artifacts associated with this work are available in the `rs-embed` project repository: `https://github.com/GISWLH/rs-embed`.

Acknowledgments

The author acknowledges the public remote sensing and Earth observation model communities whose released models, data products, and documentation made this review and benchmark possible.

References

[1] S. Lu, J. Guo, J. R. Zimmer-Dauphinee, J. M. Nieusma, X. Wang, P. vanValkenburgh, S. A. Wernke, Y. Huo, Vision foundation models in remote sensing: A survey (2025). doi:10.1109/MGRS.2025.3541952. URL https://www.osti.gov/biblio/2573563

[2] C. Huo, K. Chen, S. Zhang, Z. Wang, H. Yan, J. Shen, Y. Hong, G. Qi, H. Fang, Z. Wang, When remote sensing meets foundation model: A survey and beyond (2025). doi:10.3390/rs17020179. URL https://www.mdpi.com/2072-4292/17/2/179

[3] Z. Huang, H. Yan, Q. Zhan, S. Yang, M. Zhang, C. Zhang, Y. Lei, Z. Liu, Q. Liu, Y. Wang, A survey on remote sensing foundation models: From vision to multimodality (2025). doi:10.48550/arXiv.2503.22081. URL https://arxiv.org/abs/2503.22081

[4] K. Wu, Y. Zhang, L. Ru, B. Dang, J. Lao, L. Yu, J. Luo, Z. Zhu, Y. Sun, J. Zhang, Q. Zhu, J. Wang, M. Yang, J. Chen, Y. Zhang, Y. Li, A semantic-enhanced multi-modal remote sensing foundation

model for earth observation, Nature Machine Intelligence 7 (2025) 1235–1249. doi:10.1038/s42256-025-01078-8.
URL https://www.nature.com/articles/s42256-025-01078-8

[5] C. F. Brown, M. R. Kazmierski, V. J. Pasquarella, W. J. Rucklidge, M. Samsikova, C. Zhang, E. Shelhamer, E. Lahera, O. Wiles, S. Ilyushchenko, N. Gorelick, L. L. Zhang, S. Alj, E. Schechter, S. Askay, O. Guinan, R. Moore, A. Boukouvalas, P. Kohli, An embedding field model for accurate and efficient global mapping from sparse label data (2025).
URL https://arxiv.org/abs/2507.22291

[6] Z. Feng, C. Atzberger, S. Jaffer, J. Knezevic, S. Sormunen, R. Young, M. C. Lisaius, M. Immitzer, J. Ball, D. A. Coomes, A. Madhavapeddy, A. Blake, S. Keshav, Temporal embeddings of surface spectra for earth representation and analysis (2026).
URL https://arxiv.org/abs/2506.20380v4

[7] M. Castelluccio, G. Poggi, C. Sansone, L. Verdoliva, Land use classification in remote sensing images by convolutional neural networks, in: arXiv preprint arXiv:1508.00092, 2015.
URL https://arxiv.org/abs/1508.00092

[8] N. Gorelick, M. Hancher, M. Dixon, S. Ilyushchenko, D. Thau, R. Moore, Google earth engine: Planetary-scale geospatial analysis for everyone, Remote Sensing of Environment 202 (2017) 18–27. doi:10.1016/j.rse.2017.06.031.
URL https://www.sciencedirect.com/science/article/pii/S0034425717302900

[9] O. Mañas, A. Lacoste, X. G. i Nieto, D. Vázquez, P. Rodríguez, Seasonal contrast: Unsupervised pre-training from uncurated remote sensing data, in: ICCV, 2021.
URL https://arxiv.org/abs/2103.16607

[10] A. Dosovitskiy, L. Beyer, A. Kolesnikov, D. Weissenborn, X. Zhai, T. Unterthiner, M. Dehghani, M. Minderer, G. Heigold, S. Gelly, J. Uszkoreit, N. Houlsby, An image is worth 16x16 words: Transformers for image recognition at scale, in: ICLR, 2021.
URL https://arxiv.org/abs/2010.11929

[11] Y. Bian, J. Tao, J. Xu, X. Lu, J. Kwan, Y. hsiang Tseng, Vision transformer for remote sensing image classification, Remote Sensing 13 (3) (2021) 516. doi:10.3390/rs13030516.
URL https://www.mdpi.com/2072-4292/13/3/516

[12] Y. Cong, S. Khanna, C. Meng, P. Liu, E. Rozi, Y. He, M. Burke, D. B. Lobell, S. Ermon, Pre-training transformers for temporal and multispectral satellite imagery (2022).
URL https://arxiv.org/abs/2207.08051

[13] C. J. Reed, R. Gupta, S. Li, S. Brockman, C. Funk, B. Clipp, K. Keutzer, S. Candido, M. Uyttendaele, T. Darrell, A scale-aware masked autoencoder for multiscale geospatial representation learning (2023).
URL https://arxiv.org/abs/2212.14532

[14] F. Liu, D. Chen, Z. Guan, X. Zhou, J. Zhu, Q. Ye, L. Fu, J. Zhou, A vision language foundation model for remote sensing (2024).
URL https://arxiv.org/abs/2306.11029

[15] J. Jakubik, S. Roy, C. E. Phillips, P. Fraccaro, D. Godwin, B. Zadrozny, D. Szwarcman, C. Gomes, G. Nyirjesy, B. Edwards, D. Kimura, N. Simumba, L. Chu, S. K. Mukkavilli, D. Lambhate, K. Das, R. Bangalore, D. Oliveira, M. Muszynski, K. Ankur, M. Ramasubramanian, I. Gurung, S. Khallaghi, H. Li, M. Cecil, M. Ahmadi, F. Kordi, H. Alemohammad, M. Maskey, R. Ganti, K. Weldemariam, R. Ramachandran, Foundation models for generalist geospatial artificial intelligence (2023).
URL https://arxiv.org/abs/2310.18660

[16] Z. Xiong, Y. Wang, F. Zhang, A. J. Stewart, J. Hanna, D. Borth, I. Papoutsis, B. L. Saux, G. Camps-Valls, X. X. Zhu, Neural plasticity-inspired multimodal foundation model for earth observation (2024).
URL https://arxiv.org/abs/2403.15356

[17] G. Tseng, A. Fuller, M. Reil, H. Herzog, P. Beukema, F. Bastani, J. R. Green, E. Shelhamer, H. Kerner, D. Rolnick, Learning global & local features of many remote sensing modalities (2025).
URL https://arxiv.org/abs/2502.09356

[18] R. Ramachandran, S. Roy, M. Maskey, D. Szwarcman, P. Fraccaro, A primer for assessing foundation models for earth observation, nASA

Technical Reports Server preprint (2025).
URL https://ntrs.nasa.gov/citations/20250005271

[19] M. Noman, M. Naseer, H. Cholakkal, R. M. Anwer, S. Khan, F. S. Khan, Rethinking transformers pre-training for multi-spectral satellite imagery (2024).
URL https://arxiv.org/abs/2403.05419

[20] X. Li, Y. Tao, S. Zhang, S. Liu, Z. Xiong, C. Luo, L. Liu, M. Pechenizkiy, X. X. Zhu, T. Huang, Reobench: Benchmarking robustness of earth observation foundation models (2025). doi:10.48550/arXiv.2505.16793.
URL https://arxiv.org/abs/2505.16793

[21] Y. Wang, Z. Xiong, C. Liu, A. J. Stewart, T. Dujardin, N. I. Bountos, A. Zavras, F. Gerken, I. Papoutsis, L. Leal-Taixe, X. X. Zhu, Towards a unified copernicus foundation model for earth vision (2025).
URL https://arxiv.org/abs/2503.11849

[22] R. Daroya, E. Cole, O. M. Aodha, G. V. Horn, S. Maji, Learning satellite image representations from wildlife observations (2025).
URL https://arxiv.org/abs/2412.14428

[23] G. Astruc, N. Gonthier, C. Mallet, L. Landrieu, One earth observation model for many resolutions, scales, and modalities (2025).
URL https://arxiv.org/abs/2412.14123

[24] M. S. Danish, M. A. Munir, S. R. A. Shah, M. H. Khan, R. M. Anwer, J. Laaksonen, F. S. Khan, S. Khan, A scalable foundation model for unified multisensor earth observation (2026).
URL https://arxiv.org/abs/2506.06281

[25] J. Jakubik, F. Yang, B. Blumenstiel, E. Scheurer, R. Sedona, S. Maurogiovanni, J. Bosmans, N. Dionelis, V. Marsocci, N. Kopp, R. Ramachandran, P. Fraccaro, T. Brunschwiler, G. Cavallaro, J. Bernabe-Moreno, N. Longepe, Large-scale generative multimodality for earth observation (2025).
URL https://arxiv.org/abs/2504.11171

[26] W. Li, S. Liang, K. Chen, Y. Chen, H. Ma, J. Xu, Y. Ma, Y. Zhang, S. Guan, H. Fang, Z. Shi, Agrifm: A multi-source temporal remote

sensing foundation model for agriculture mapping (2026).
URL https://www.sciencedirect.com/science/article/pii/S0034425726000040

[27] N. I. Bountos, A. Ouaknine, I. Papoutsis, D. Rolnick, Multi-modal, multi-scale and multi-task remote sensing foundation models for forest monitoring (2025).
URL https://arxiv.org/abs/2312.10114

[28] T. Forgaard, J. Reksten, A. Waldeland, V. Marsocci, N. Longepe, M. Kampffmeyer, A.-B. Salberg, A versatile foundation model for earth observation climate and society applications (2026).
URL https://arxiv.org/abs/2601.16011

[29] C. S. Spradlin, J. A. Caraballo-Vega, J. Li, M. L. Carroll, J. Gong, P. M. Montesano, A geospatial foundation model for coarse-resolution all-sky remote sensing imagery (2024).
URL https://arxiv.org/abs/2411.17000

[30] L. Ma, Y. Liu, X. Zhang, Y. Ye, G. Yin, B. A. Johnson, Deep learning in remote sensing applications: A meta-analysis and review, ISPRS Journal of Photogrammetry and Remote Sensing 152 (2019) 166–177. doi:10.1016/j.isprsjprs.2019.04.015.

[31] Q. Yuan, H. Shen, T. Li, Z. Li, S. Li, Y. Jiang, H. Xu, W. Tan, Q. Yang, J. Wang, J. Gao, L. Zhang, Deep learning in environmental remote sensing: Achievements and challenges, Remote Sensing of Environment 241 (2020) 111716. doi:10.1016/j.rse.2020.111716.

[32] M. Weiss, F. Jacob, G. Duveiller, Remote sensing for agricultural applications: A meta-review, Remote Sensing of Environment 236 (2020) 111402. doi:10.1016/j.rse.2019.111402.

[33] M. E. Paoletti, J. M. Haut, J. Plaza, A. Plaza, Deep learning classifiers for hyperspectral imaging: A review, ISPRS Journal of Photogrammetry and Remote Sensing 158 (2019) 279–317. doi:10.1016/j.isprsjprs.2019.09.006.

[34] K. Li, G. Wan, G. Cheng, L. Meng, J. Han, Object detection in optical remote sensing images: A survey and a new benchmark, ISPRS Journal

of Photogrammetry and Remote Sensing 159 (2020) 296–307. doi:10.1016/j.isprsjprs.2019.11.023.

[35] A. Xiao, W. Xuan, J. Wang, J. Huang, D. Tao, S. Lu, N. Yokoya, Foundation models for remote sensing and earth observation: A survey, IEEE Geoscience and Remote Sensing Magazine (2025). doi:10.1109/MGRS.2025.3576766.

[36] G. Cheng, J. Han, A survey on object detection in optical remote sensing images, ISPRS Journal of Photogrammetry and Remote Sensing 117 (2016) 11–28. doi:10.1016/j.isprsjprs.2016.03.014.

[37] D. Szwarcman, S. Roy, P. Fraccaro, T. E. Gislason, B. Blumenstiel, R. Ghosal, P. H. de Oliveira, J. L. de Sousa Almeida, Prithvi-eo-2.0: A versatile multitemporal foundation model for earth observation applications, IEEE Transactions on Geoscience and Remote Sensing (2026). doi:10.1109/TGRS.2025.3642610.

[38] X. Li, C. Li, P. Ghamisi, D. Hong, J. A. Benediktsson, J. Chanussot, Fleximo: A flexible remote sensing foundation model, IEEE Transactions on Geoscience and Remote Sensing (2026). doi:10.1109/TGRS.2026.3656362.